Controlled Quantum Semantic Communication for Industrial CPS Networks

Syed Muhammad Abuzar Rizvi, Uman Khalid, Symeon Chatzinotas, *Fellow, IEEE*, Trung Q. Duong, *Fellow, IEEE*, and Hyundong Shin, *Fellow, IEEE*

***Abstract*—Computing-intensive semantic communication emphasizes context, enabling the extraction of task-specific semantics from the source data and the reconstruction of the intended meaning at the destination. In industrial cyber-physical systems (CPSs), this approach can optimize automation processes while minimizing communication overhead with efficient bandwidth use in environments where machines, sensors, and controllers must communicate frequently. By integrating quantum communication with computing-empowered semantic methods, we can achieve unprecedented efficiency and security in task-oriented data transmission, effectively safeguarding against eavesdropping and other attacks. This paper presents a controlled quantum semantic communication (QSC) framework that leverages semantic extraction for anomaly detection in industrial CPS networks and employs controlled quantum communication to send the data securely with high semantic fidelity. A machine learning model extracts semantic information from images as the hull point data representing defective regions as pixel points. This data is then transmitted with high fidelity using quantum communication with controlled quantum state preparation. We use discrete- and continuous-variable states to simulate quantum binary phase-shift keying (BPSK) and M-ary pulse position modulation (M-PPM), respectively. At the receiver, these quantum states are measured using optimal quantum decision-making and converted back into the hull point data, thereby generating the anomaly map. This map is overlaid on a template image to highlight defect positions, which can be used for industrial quality control. Furthermore, we simulate the controlled QSC framework (BPSK and M-PPM) across a diverse set of anomaly detection examples and evaluate the QSC performance in industrial CPS networks.**

***Index Terms*—Industrial anomaly detection, machine learning, quantum semantic communications, quantum control.**

The fundamental research described in this paper was supported, in part, by the National Research Foundation of Korea (NRF) grant funded by the Korean government (MSIT) (RS-2025-00556064), by the MSIT (Ministry of Science and ICT), Korea, under the ITRC (Information Technology Research Center) support program (IITP-2025-2021-0-02046) supervised by the IITP (Institute for Information & Communications Technology Planning & Evaluation), by the project Lux4QCI under Grant GA 101091508 funded by the Digital Europe Program, by the project LUQCIA funded by the Government of Luxembourg/SMC, and by the Canada Excellence Research Chair (CERC) Program CERC-2022-00109. *(Corresponding author: Hyundong Shin.)*

S. M. A. Rizvi, U. Khalid, and H. Shin are with the Department of Electronics and Information Convergence Engineering, Kyung Hee University, 1732 Deogyeong-daero, Giheung-gu, Yongin-si, Gyeonggi-do 17104 Korea (e-mail: hshin@khu.ac.kr).

S. Chatzinotas is with the Interdisciplinary Centre for Security, Reliability, and Trust, University of Luxembourg, 1855 Luxembourg City, Luxembourg (e-mail: symeon.chatzinotas@uni.lu).

T. Q. Duong is with the Faculty of Engineering and Applied Science, Memorial University, St. John's, NL A1C 5S7, Canada, and is also with the School of Electronics, Electrical Engineering and Computer Science, Queen's University Belfast, Belfast, U.K. (e-mail: tduong@mun.ca).

I. Introduction

DIGITAL transformation in industrial automation, driven by advancements in the industrial Internet of Things (IoT) and cyber-physical systems (CPSs), has fundamentally transformed the way industries operate. Smart factories are no longer reliant on rigid, predefined processes but instead are characterized by their ability to respond dynamically to real-time data [1]–[4]. This transformation is driven by the integration of artificial intelligence (AI), machine learning (ML), and cloud-fog computing, which collectively support the efficient management of vast, interconnected networks of devices [5], [6]. These technologies empower predictive maintenance, process optimization, and adaptive control, allowing industrial IoT and CPS networks to operate more intelligently and autonomously than ever before. However, this increased connectivity and intelligence bring new challenges, particularly in terms of communication efficiency, security, and system adaptability, as the complexity of managing real-time data across diverse devices continues to grow.

One of the critical challenges in this evolving industrial landscape is ensuring that communication between numerous interconnected devices and sensors remains both efficient and secure [7], [8]. Traditional models, such as the International Society of Automation (ISA)-95, which have long served as the backbone of industrial automation, are now being re-evaluated. The growing need for real-time data processing and rapid decision-making calls for more flexible and dynamic communication frameworks that can adapt to the complexities of modern industrial environments (ISA-95 models) [9]. In response to these challenges, the semantic communication framework has emerged as a promising solution. By transmitting the meaning of data rather than just raw bits, semantic communication enhances the efficiency and effectiveness of information exchange in industrial environments [10]–[13]. Traditional communication systems prioritize delivering data accurately, but semantic communication ensures that the essential information is correctly understood at the receiver end. For example, in a smart factory, sensors generate large volumes of data that need to be processed and communicated to various components for effective decision-making. With semantic communication, only the essential information (e.g., patterns indicating machine failures or production bottlenecks) is transmitted, reducing bandwidth usage and improving communication efficiency. By filtering out redundant or non-critical data, semantic communication ensures that only the most relevant information is received, enabling faster and more

TABLE I
EXPANSIONS OF IMPORTANT ACRONYMS

Acronym	Expansion	Acronym	Expansion
BB84	Bennett and Brassard 1984	BPSK	Binary Phase-Shift Keying
CRAB	Chopped Random-Basis	CPS	Cyber-Physical Systems
CV	Continuous Variable	DEP	Decision Error Probability
DL	Deep Learning	DQL	Deep Q-learning
DRL	Deep Reinforcement Learning	DV	Discrete Variable
GRAPE	Gradient Ascent Pulse Engineering	ML	Machine Learning
mIoU	Mean Intersection over Union	M-PPM	M-ary Pulse Position Modulation
NMSE	Normalized Mean Squared Error	NISQ	Noisy Intermediate-Scale Quantum
QAT	Quantum Anonymous Teleportation	QKD	Quantum Key Distribution
QML	Quantum Machine Learning	QOC	Quantum Optimal Control
QSC	Quantum Semantic Communication	RL	Reinforcement Learning
SC	Semantic Communication	SSIM	Structural Similarity Index Measure

informed decision-making.

As industrial systems evolve, the demand for more robust and secure communication frameworks becomes increasingly critical. The growing reliance on cloud-fog architectures, where data processing and decision-making are distributed across multiple layers, introduces unique challenges in ensuring data integrity and secure transmission [6], [14]. Advanced AI-driven models used in industrial inspection systems require vast amounts of real-time data to operate effectively, yet this also heightens their vulnerability to cyber-attacks. While effective, traditional encryption methods may not be sufficient to protect against the sophisticated threats targeting modern industrial infrastructures [15]. As industries become increasingly interconnected and data-centric, ensuring secure communication and protecting critical operations have become paramount [16]–[18].

Recently, quantum information science has gained a lot of popularity due to its potential to revolutionize computing, communication, and cryptography. With advancements in quantum algorithms, error correction, and qubit technology, researchers are exploring ways to harness quantum mechanics for solving complex problems far beyond the reach of classical computers while also enhancing areas of machine learning [19], [20], optimization [21], [22], sensing [23] and beyond [24]. The integration of quantum communication with semantic frameworks introduces a revolutionary dimension of security to industrial systems. Quantum communication leverages the principles of quantum mechanics, such as the no-cloning theorem, to establish secure channels for data transmission, making them nearly impervious to conventional hacking methods [25]–[27]. If an eavesdropper attempts to intercept the information, the quantum state of the communication particles is disturbed, immediately alerting the parties to the intrusion [28], [29]. This inherent security mechanism ensures that any unauthorized access is instantly detectable, making quantum communication virtually immune to eavesdropping and man-in-the-middle attacks. In environments where sensitive and mission-critical data is continuously exchanged between interconnected devices, such as in predictive maintenance or real-time anomaly detection, this additional layer of security is essential. By securing both the semantic content [30] and the transmission channel using quantum protocols [31], [32], industries can ensure that their communication systems not only transmit critical information efficiently but also protect it from emerging cybersecurity threats using quantum semantic communication (QSC).

State preparation is a critical challenge for achieving a low error rate in quantum communication systems. In discrete-variable (DV) quantum systems, high-fidelity quantum states are required to preserve the integrity of transmitted information, as even small deviations can lead to significant errors during transmission [29], [33], [34]. Quantum optimal control (QOC) addresses this issue by determining the optimal control functions or pulses that steer the system to the desired quantum state with maximum precision. When applied to quantum communication, this optimal control ensures that the quantum states encoding the information are transmitted with minimal distortion, thereby preserving the reliability and accuracy of the communication process. In continuous-variable (CV) quantum systems, coherent states of the electromagnetic field are widely utilized in quantum communication protocols. These coherent states are typically generated by lasers or other highly controlled light sources, which are characterized by the average number of photons. In quantum communication modulations such as quantum on-off keying and M-ary pulse position modulation (M-PPM), increasing the average number of photons reduces the error probability [33]. Using pulse control, quantum systems can be controlled to prepare coherent states by manipulating the control function. In industrial applications, where communication networks often operate under strict performance and error-rate constraints, the use of control alongside quantum communication ensures that critical data is transmitted securely with exceptionally low error rates. This is especially critical in environments that require real-time, high-precision operations, such as in automated manufacturing systems or real-time industrial monitoring, where even minor communication errors could result in costly system malfunctions or downtime. By improving the fidelity of quantum state preparation, control plays a vital role in ensuring that quantum communication systems meet the stringent demands of modern

industrial processes.

In the paper, we propose a controlled QSC framework comprising two main components: semantic extraction with reconstruction and quantum state control during communication. The method leverages ML for the semantic extraction and reconstruction of industrial data, particularly in the context of anomaly detection in image-based industrial inspection systems. This framework employs FastFlow [35], an ML model specifically designed for fast and accurate anomaly detection in image-based tasks, such as defect detection in industrial settings. Given an input image of any manufactured product, the model highlights regions where potential defects are located. These regions are then translated into the hull point data, which consists of key pixel coordinates outlining the boundary of the defective area. This data is then converted into its binary representation for transmission using quantum communication. For DV quantum states, we employ quantum binary phase-shift keying (BPSK), where each binary bit is mapped into a quantum state with a phase shift depending on the bit value. The QOC methods are utilized for quantum state preparation to ensure high-fidelity communication, preserving the accuracy of the transmitted data. The QOC optimizes the control function and operations used to manipulate quantum systems. Herein, we employ three QOC methods: chopped random-basis (CRAB) [36], gradient ascent pulse engineering (GRAPE) [37], [38], and deep Q-learning (DQL) [39], [40]. For CV states, we utilize quantum M-PPM where data is mapped as the position of a coherent state using a pulse symbol. This coherent state is characterized by the average number of photons present, while the vacuum state contains none. To prepare these quantum states, we apply control to a quantum dot system, which can generate photons upon excitation by a pulse [41]. Using precise pulse control, we can increase the probability of photon emission, making quantum M-PPM communication more robust. At the receiver end, using optimal quantum decision-making, quantum states are decoded back into the hull point data, generating the anomaly map. This map is then overlayed onto a template image, highlighting the detected area of the original image. This controlled QSC conveys the semantics of the defective region of the manufactured object in an efficient and secure way, as required in automated industrial CPS networks.

The rest of this paper is organized as follows. Section III explores applications for semantic communication in industrial CPS networks and discusses anomaly semantic extraction and reconstruction. Sections IV and V detail the controlled DV and CV QSC frameworks for industrial anomaly detection. Finally, Section VI gives a brief conclusion. Important acronyms are summarized in Table I.

II. Literature Reviews

Traditional communication, rooted in Shannon's model, focuses on maximizing bit rates and minimizing noise-induced errors [42]. However, with the increasing demands of 6G networks, autonomous systems, and human-machine interaction, this approach becomes insufficient. Semantic communication (SC) shifts the focus to transmitting only task-relevant information, thereby significantly reducing resource usage. This reduction in transmitted information ultimately alleviates bandwidth constraints and latency issues. Recently, quantum communication and quantum computing have attracted considerable attention owing to their unique advantages rooted in quantum phenomena—such as entanglement, superposition, no-cloning, and parallelism—which offer superior capabilities in computation, security, and sensing compared to classical systems [43]. Notable protocols such as quantum key distribution (QKD) and quantum anonymous communication (QAC) provide enhanced encryption, anonymity, and privacy, ensuring quantum-safe security [44], [45]. The advantages offered by quantum information science can be integrated into SC to form QSC. This QSC encompasses multiple paradigms such as classical semantic extraction with quantum communication, quantum semantic extraction using quantum machine learning (QML) with classical communication, and quantum semantic extraction with quantum communication. In this section, we provide a brief overview of various QSC approaches.

One of the earliest QSC frameworks was proposed in [46], leveraging quantum embedding, high-dimensional Hilbert spaces, and QML techniques, such as quantum clustering, to construct minimalist, efficient, and accurate semantic representations. The authors demonstrated that incorporating semantic information reduces quantum resource consumption compared to conventional quantum communication systems. Building on this work, [47] focused on resource-efficient designs, introducing models that achieve semantic compression to minimize quantum resource usage. Focusing on the communication layer, [13] proposed a sustainable quantum semantic broadcast framework. This system integrates foundation models for semantic extraction with QAC protocols, employing model pruning and distillation techniques to reduce computational complexity while ensuring quantum-safe broadcasting via anonymous entanglement. Similarly, [48] introduced a pragmatic SC framework over quantum channels, targeting efficient and robust knowledge transmission. By integrating pre-trained large language models and graph neural networks for semantic encoding, and employing remote state preparation for quantum transmission, the framework maintains high semantic fidelity even under depolarizing and dephasing noise. A Metaverse-oriented case study in [49] presented a QSC architecture tailored for immersive environments. This framework encodes semantic content into quantum states using variational quantum circuits and transmits them via quantum anonymous teleportation (QAT). The use of geometrically uniform quantum states and square-root measurements improves resilience to noise while preserving semantic meaning.

Collectively, these studies highlight the QSC's versatility and promise in redefining how systems communicate meaning. The QSC system not only promises to significantly reduce communication overhead and ensure quantum-level security but also introduces a new framework for contextual reasoning and goal-driven interaction in AI-native quantum networks. However, several challenges remain—particularly in hardware scalability, noisy intermediate-scale quantum (NISQ) device limitations [50], and the lack of standardized metrics for evaluating quantum semantic fidelity and contextual expressiveness.

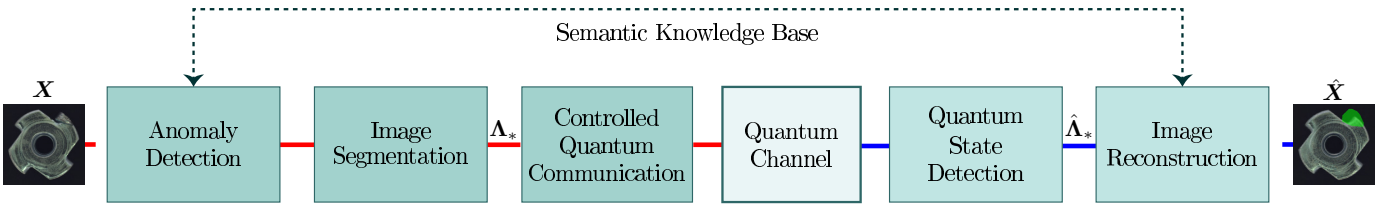

Fig. 1. A controlled QSC system for image-based anomaly detection in industrial CPS networks. Input images from industrial sensors are processed using ML methods to extract relevant semantic representations, which are then encoded into quantum states and transmitted over a quantum channel with enhanced fidelity using QOC techniques.

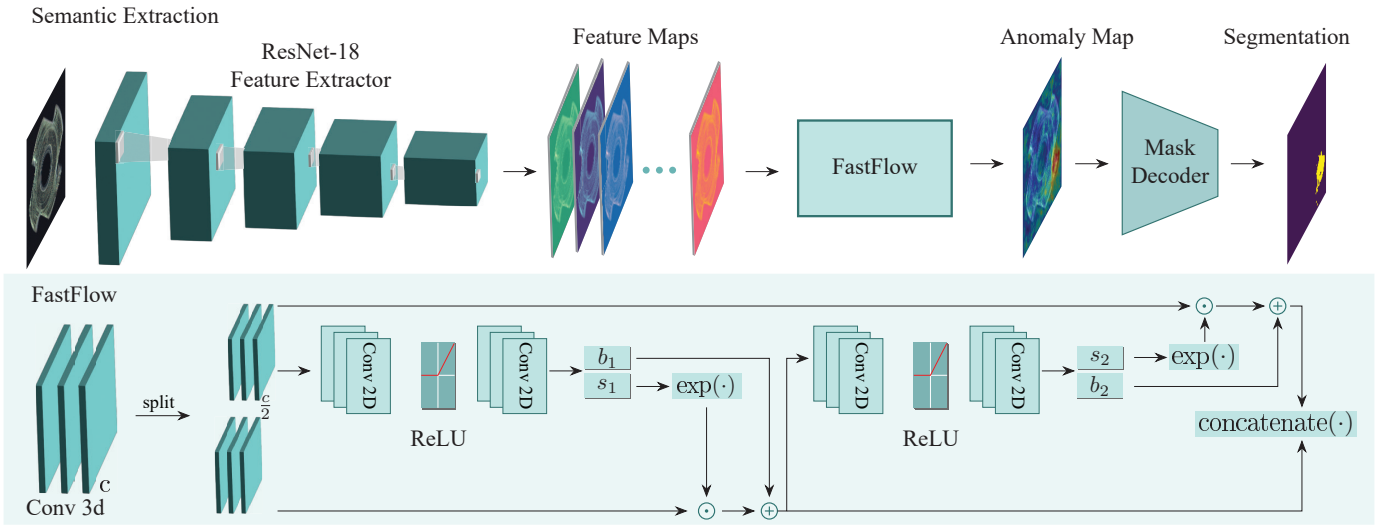

Fig. 2. Semantic anomaly detection with FastFlow. A semantic extraction pipeline using ResNet-18 generates feature maps from input images, followed by FastFlow for anomaly map generation and mask decoding for segmentation. A detailed architecture of the FastFlow modules is also depicted where convolutions are applied to split feature maps, followed by nonlinear transformations (ReLU) and exponential scaling to compute anomaly scores, which are subsequently concatenated for final segmentation.

III. Semantic Communication for Industrial CPSs

We present a controlled QSC framework designed to extract semantic information from images and transmit it using quantum states, enabling secure and semantically rich information exchange for anomaly detection. The protocol framework is illustrated in Fig. 1. Semantic communication has the potential to greatly improve the performance of industrial CPSs. Traditional communication systems transmit data without considering the semantic content, leading to inefficiencies and potential vulnerabilities. In contrast, semantic communication focuses on the meaning and context of the data, ensuring that only relevant and necessary information is transmitted. This approach can reduce communication overhead and improve communication efficiency in industrial CPS networks.

A. CPS Applications

1) Defect Detection in Manufacturing: In defect detection within manufacturing [51]–[55], semantic communications can optimize the data transmission process by focusing on transmitting only the most relevant information. Instead of sending entire image datasets, which are often large and resource-intensive, semantic communication systems can leverage deep learning (DL) models to identify and extract critical features that indicate potential defects. These features may include anomalies, irregularities, or patterns that are indicative of issues in the manufacturing process. Once identified, the system can isolate and prioritize data transmission from pixel regions most likely to contain defects, significantly reducing the volume of data that needs to be sent. This targeted approach allows for faster processing and decision-making, enabling (near) real-time defect detection. By concentrating only on the essential data, semantic communication conserves bandwidth, reduces latency, and enhances the overall efficiency of automated quality control systems in manufacturing.

2) Automated Sorting Systems: In automated sorting systems, especially in industries such as logistics, recycling, and agriculture, accurate and efficient image segmentation is crucial for distinguishing between different types of items or materials [56], [57]. Semantic communication plays a vital role in improving the performance of these systems by ensuring that only the most relevant segmented data is processed and transmitted. Traditional image-based sorting systems often need to handle large volumes of high-resolution data, which can slow down operations and introduce latency in decision-making. However, with semantic communications, DL models can perform image segmentation, isolating key features or

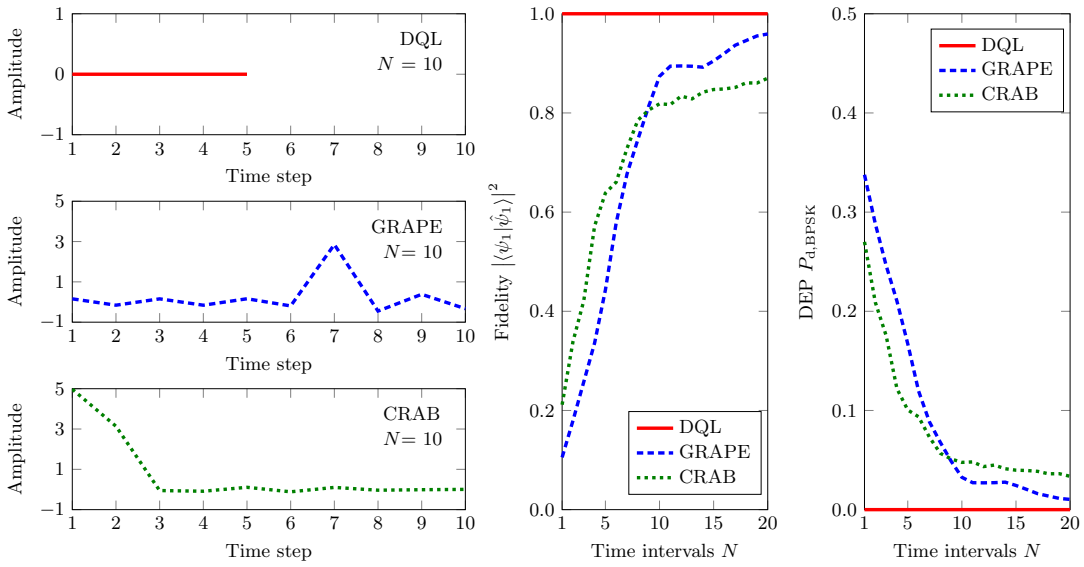

Fig. 3. Controlled pulse amplitudes, quantum state fidelity, and DEP for BPSK QSC with DQL, GRAPE, and CRAB qubit control. Controlled pulse amplitudes are plotted for 10 time intervals ($N = 10$) at each time interval in T (left). Quantum state fidelity $\left|\langle\psi_1|\hat{\psi}_1\rangle\right|^2$ and DEP $P_{\mathrm{d,BPSK}}$ are also depicted as a function of time intervals N (right).

characteristics necessary for sorting, such as shape, size, color, or texture. Instead of transmitting the entire image, the system can identify the critical segments required for accurate sorting and prioritize their transmission. By focusing on the most relevant segments, the system reduces bandwidth requirements, enabling low-latency communication between sensors, processors, and actuators. This streamlined data flow not only accelerates sorting operations but also improves precision by minimizing errors associated with processing large amounts of unnecessary data.

3) Vision-Based Worker Monitoring: Semantic communication enables networks to dynamically adapt to human actions in real time, offering significant safety and efficiency improvements in environments where humans and machines work closely together. A key application of semantic communication in such settings is the detection and response to safety-critical situations. Instead of merely analyzing raw data streams from sensors or cameras, semantic systems interpret the meaning behind the data. For example, if a worker is detected near a hazardous area or in an unsafe posture, the network can prioritize this information, alerting both the worker and relevant machinery to prevent accidents [58]. This real-time hazard detection and response capability allows for rapid interventions, reducing the likelihood of injuries and equipment damage. Additionally, semantic communication can ensure compliance with safety regulations, such as the wearing of personal protective equipment. By analyzing visual and sensor data, the network can automatically detect whether workers are wearing required safety gear, such as helmets, gloves, or high-visibility clothing. If any safety gear is missing or improperly worn, the network can promptly alert the operator or supervisor, enabling swift corrective actions. This automated monitoring reduces human error and helps maintain a consistently safe working environment.

B. Anomaly Semantic Extraction and Reconstruction

The problem of unsupervised anomaly detection involves identifying and localizing anomalies in images where only normal data is available during training. The critical challenge is to detect deviations from the expected patterns in new, unseen images by modeling the feature distribution of normal data and identifying outliers that do not conform to this distribution. This approach enables effective anomaly detection without requiring labeled anomaly examples. In this paper, we employ a two-dimensional normalizing flow-based probability distribution estimator known as Fastflow [35].

Let $\boldsymbol{X} \in \mathbb{R}^{h\times w\times 3}$ be an input image with RGB channels, where h and w denote the image height and width, respectively. Then, FastFlow initiates by extracting a feature map $\boldsymbol{Y} \in \mathbb{R}^{h'\times w'\times c}$ from the input image $\boldsymbol{X}$ using a deep feature extractor, known as the backbone model, such as ResNet or Vision Transformer, where c denotes the number of feature channels. Subsequently, FastFlow applies a two-dimensional normalizing flow model to transform the feature map $\boldsymbol{Y}$ into a latent representation $\boldsymbol{Z} \in \mathbb{R}^{h'\times w'}$ that conforms to the standard Gaussian distribution. The anomaly score λ_{ij} for the (i,j)th pixel in the feature map is now computed by evaluating the negative log-likelihood of its corresponding latent variable z_{ij} under the standard Gaussian distribution as follows:

$$\lambda_{ij} = -\log\left(\frac{1}{\sqrt{2\pi}}e^{-z_{ij}^2/2}\right) \tag{1}$$

leading to a two-dimensional anomaly score map $\boldsymbol{\Lambda} \in \mathbb{R}^{h'\times w'}$. This anomaly score map $\boldsymbol{\Lambda}$ is then upsampled to match the original image dimension $h \times w$, often using bilinear interpolation or similar techniques, yielding the final anomaly segmentation map $\boldsymbol{\Lambda}_* \in \mathbb{R}^{h\times w}$.

The final segmentation map $\boldsymbol{\Lambda}_*$ provides a pixel-wise anomaly score, where each pixel value quantifies the likelihood of that region deviating from the learned Gaussian

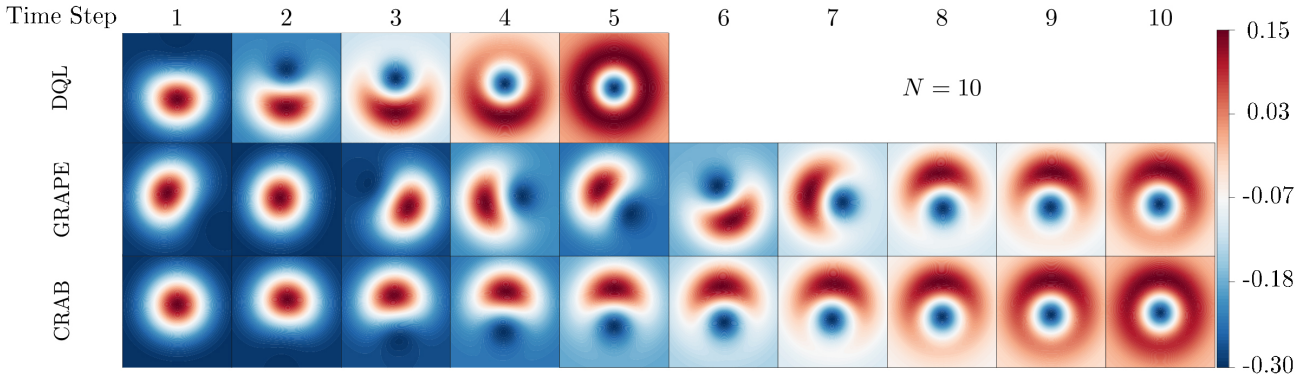

Fig. 4. Wigner function of state evolution from $|\psi_0\rangle$ to $|\psi_1\rangle$ at each control interval in T for DQL, GRAPE, and CRAB qubit control when $N = 10$.

distribution, effectively indicating potential anomalies. The overall framework of the model is illustrated in Fig. 2. The largest area of the segmentation map $\mathbf{\Lambda}_*$ can be interpreted as a contour that highlights the defective region of the product. Let $\mathcal{S}$ be the set of points along the contour of $\mathbf{\Lambda}_*$. A convex hull algorithm is then applied to the set $\mathcal{S}$ to obtain the set $\mathcal{P}$ of convex hull points, forming a convex polygon using edge detection and contour extraction [59]. The number of hull points determines the geometric complexity and fidelity of the convex boundary representing a shape. A small number of hull points simplifies the contour, potentially losing fine details, while a large number retains more precise boundary information. In communication or compression tasks, fewer points reduce transmission costs but risk under-representing critical structures. Depending on the task, we optimize the trade-off between data efficiency and shape accuracy. This hull point data $\mathcal{P}$ is converted into binary data $\mathcal{B}$. These binary values are then mapped into quantum states for transmission. At the receiver end, the reconstructed hull point data $\hat{\mathcal{P}}$ is used to regenerate the defect region on a template image, producing the output image $\hat{\boldsymbol{X}}$, which retains the same semantic information as the image after anomaly detection.

IV. Controlled DV QSC for Anomaly Detection

Quantum communication offers significantly enhanced security compared to classical systems by leveraging fundamental principles of quantum mechanics. Unlike classical methods, which rely on computational hardness assumptions, quantum protocols derive security from physical laws such as entanglement, state collapse, and the no-cloning theorem [33]. Since any measurement inevitably disturbs a quantum state, eavesdropping can be detected through observable error rates, as demonstrated in the Bennett and Brassard 1984 (BB84) protocol [60]. Consequently, intercepting data exchanged between industrial CPS sensors, controllers, and actuators becomes exceedingly difficult within the QSC framework. Furthermore, quantum states cannot be copied without introducing detectable errors, unlike classical data, which can be replicated and stored indefinitely without disruption [61]. This fundamental difference effectively mitigates replay attacks—where previously captured valid data packets are resent to deceive CPS components into executing outdated or malicious commands.

Building upon these inherent properties, QSC can incorporate advanced quantum protocols to guarantee anonymity and privacy, surpassing the capabilities of classical communication systems [27], [62], [63]. For instance, the QAT protocol enables semantics-aware NISQ devices to exchange information while concealing their identities, thus eliminating the need for trusted intermediaries [64], [65]. This capability mitigates man-in-the-middle attacks, where adversaries covertly relay or alter communications, as well as identity spoofing attacks, in which malicious actors attempt to impersonate legitimate industrial CPS devices. As device identities remain hidden throughout the communication process, attackers cannot locate or impersonate target devices. Additionally, the confidentiality of semantic information is further protected by encrypting extracted semantic content using public keys established through QKD [66], providing an additional layer of security against unauthorized access. This study presents the QSC framework using fundamental quantum communication schemes such as BPSK and M-PPM, which can be extended to the aforementioned secure protocols. Our primary focus is on the challenge of quantum state preparation, rather than implementing any specific anonymity or privacy protocol.

Quantum information can be encoded and transmitted using two fundamental paradigms: DV and CV quantum states. DV systems employ finite-dimensional Hilbert spaces, encoding information typically in degrees of freedom such as photon polarization, time bin, and photon number, or the internal states of atoms and ions [67], [68]. DV protocols—including the BB84 QKD and quantum teleportation between matter qubits—are well-established for their robustness and compatibility with heralded entanglement and Bell-state measurements. In contrast, CV systems utilize infinite-dimensional Hilbert spaces, encoding information in continuous observables, such as the quadrature amplitudes of optical fields [69]. CV quantum communication leverages homodyne or heterodyne detection techniques and often employs Gaussian states (e.g., coherent and squeezed states) to implement protocols like CV-QKD [70], quantum teleportation of optical modes, and quantum sensing tasks. While DV systems provide high-fidelity control over single photons and are well suitable for

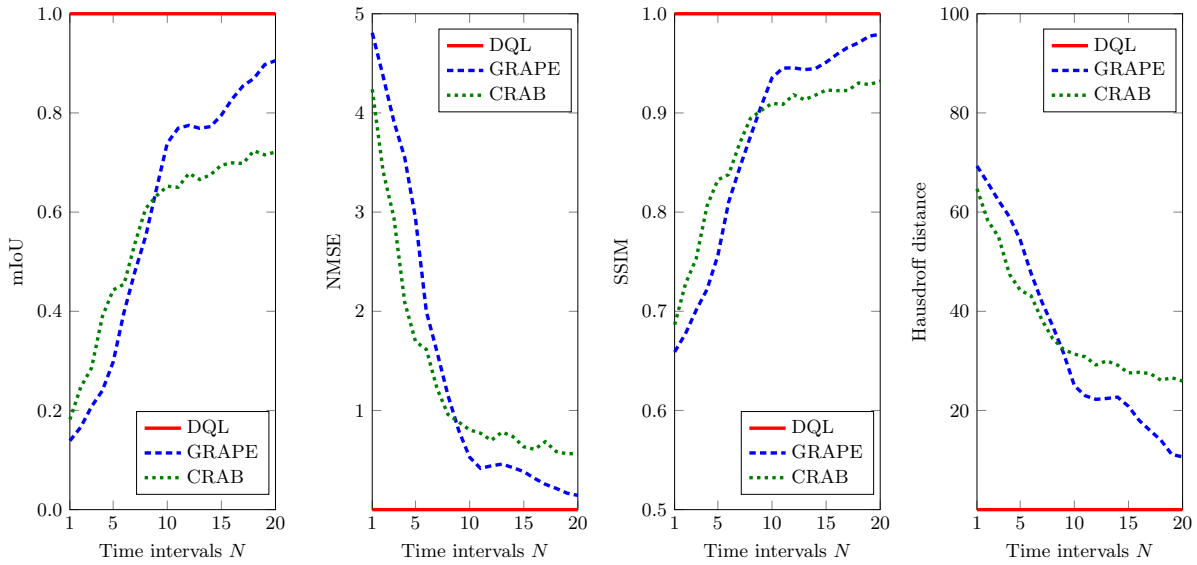

Fig. 5. mIoU, NMSE, SSIM, and Hausdorff distance for anomaly detection as a function of quantization levels N for BPSK QSC with DQL, GRAPE, and CRAB qubit control.

small to medium-scale quantum networks and repeaters, CV approaches offer advantages including high data rates, compatibility with standard wireless components, and resilience against certain losses, making them especially attractive for large-scale, fiber-based quantum communication infrastructures [71], [72]. In this section, we develop controlled DV QSC with quantum BPSK for industrial anomaly detection. By leveraging QOC, the system achieves optimal performance, effectively preserving data integrity during the transmission of hull point data extracted by anomaly detection algorithms.

A. Quantum BPSK

In the quantum BPSK, data can be represented by two distinct quantum states i.e., ground state $|0\rangle$ and its π-phase shifted state i.e., $|1\rangle$ as follows:

$$0 \rightarrow e^{\imath 0}\,|\psi_0\rangle = |\psi_0\rangle \tag{2}$$

$$1 \rightarrow e^{\imath \pi}\,|\psi_0\rangle = |\psi_1\rangle \tag{3}$$

where $\imath = \sqrt{-1}$, $|\psi_0\rangle$ can be taken as the ground state $|0\rangle$, and $|\psi_1\rangle$ can be taken as the excited state $|1\rangle$. For optimal quantum measurement, the Helstrom measurement minimizes the probability of decision error. The decision error probability (DEP) in distinguishing between the two states is given by [33]

$$P_{\mathrm{d,BPSK}} = \frac{1}{2}\left(1 - \sqrt{1 - |\langle\psi_0|\psi_1\rangle|^2}\right) \tag{4}$$

depending on the decreasing overlap between the two quantum states. For optimal quantum BPSK communication, the two states $|\psi_0\rangle$ and $|\psi_1\rangle$ must be orthogonal for optimal detection.

Assuming we can generate $|\psi_0\rangle$ without error, we want to produce its maximally orthogonal state $|\psi_1\rangle$, starting from a random state $|\hat{\psi}_1\rangle = \alpha\,|0\rangle + \beta\,|1\rangle$. Then, the inner products are given as

$$\langle\psi_0|\hat{\psi}_1\rangle = \alpha \tag{5}$$

$$\langle\psi_1|\hat{\psi}_1\rangle = \beta \tag{6}$$

Since $|\alpha|^2 + |\beta|^2 = 1$, we have

$$\left|\langle\psi_0|\hat{\psi}_1\rangle\right|^2 = 1 - \left|\langle\psi_1|\hat{\psi}_1\rangle\right|^2. \tag{7}$$

Therefore, we can rewrite (4) as

$$P_{\mathrm{d,BPSK}} = \frac{1}{2}\left(1 - \sqrt{\left|\langle\psi_1|\hat{\psi}_1\rangle\right|^2}\right). \tag{8}$$

This reveals that as the state $|\hat{\psi}_1\rangle$ approaches $|\psi\rangle_1$, the probability of error decreases, leading to optimal communication. This reduction in errors when transmitting the hull point vector results in communication with high semantic fidelity. The QOC schemes facilitate optimal state preparation for efficient communication. To send the hull point binary data $\mathcal{B}$, we can encode it into quantum states as follows:

$$\mathcal{B} \rightarrow \bigotimes_{i=1}^{|\mathcal{B}|} |b_i\rangle \tag{9}$$

where $\otimes$ denotes the tensor product and $b_i \in \{0, 1\}$ is the ith bit value of the binary data $\mathcal{B}$.

B. Controlled DV Quantum State Preparation

The QOC is a field dedicated to developing strategies and techniques for manipulating the dynamics of quantum systems to achieve specific objectives. These objectives can include preparing a particular quantum state, implementing quantum gates for quantum computing, and more. The central idea is to determine the optimal control parameters that drive the system's evolution in a desired manner. The evolution of a quantum system is typically governed by the Schrödinger equation (for closed systems), which describes the time evolution of a quantum state $|\psi(t)\rangle$ under a Hamiltonian $\boldsymbol{\mathcal{H}}(t)$ as follows:

$$\imath\hbar\frac{d}{dt}\,|\psi(t)\rangle = \boldsymbol{\mathcal{H}}(t)\,|\psi(t)\rangle \tag{10}$$

where $\hbar$ is the Planck constant. Here, $\boldsymbol{\mathcal{H}}(t)$ can be decomposed into an uncontrollable (drift) part $\boldsymbol{\mathcal{H}}_{\mathrm{d}}$ and a controllable part $\boldsymbol{\mathcal{H}}_{\mathrm{c}}$ influenced by a control function $\epsilon(t)$:

$$\boldsymbol{\mathcal{H}}(t) = \boldsymbol{\mathcal{H}}_{\mathrm{d}} + \epsilon(t)\,\boldsymbol{\mathcal{H}}_{\mathrm{c}}. \tag{11}$$

The performance of control strategies is typically quantified by an objective function $J(\boldsymbol{\theta})$, where $\boldsymbol{\theta}$ represents the evolution of control parameters. In state preparation, the objective function can be the fidelity between the final state $|\psi_{\boldsymbol{\theta}}(T)\rangle$ and the target state $|\psi_*\rangle$, leading to minimizing the infidelity objective:

$$J(\boldsymbol{\theta}) = 1 - |\langle\psi_*|\psi_{\boldsymbol{\theta}}(T)\rangle|^2. \tag{12}$$

Quantum systems employ a variety of sophisticated algorithms to optimize control parameters. Notable among these are CRAB [36], GRAPE [37], [38], DQL based on reinforcement learning (RL) [39], [40], stochastic gradient descent [73], and Krotov's method [38], [74]. In this paper, we employ these techniques—namely, CRAB, GRAPE, and DQL.

1) CRAB: The CRAB method for QOC is to find optimal control pulses that guide a quantum system to a desired target state. The main idea is to express the control function $\epsilon(t)$ as the sum of a predefined guess function and K weighted sine and cosine functions of randomly chosen frequencies. This expansion allows the optimization process to explore a broad and flexible space of control solutions. By adjusting the $2K$ weighting coefficients, the CRAB method aims to optimize the objective function as in (12). The randomization of the frequencies helps the method avoid local minima and achieve more effective control in complex quantum systems.

2) GRAPE: The gradient $\partial J(\boldsymbol{\theta})/\partial\epsilon(t)$ of the objective function with respect to the control function $\epsilon(t)$ is used to iteratively update $\epsilon(t)$ in the GRAPE method as follows:

$$\epsilon(t) \leftarrow \epsilon(t) - \delta\frac{\partial J(\boldsymbol{\theta})}{\partial\epsilon(t)} \tag{13}$$

where δ is a small step size determining the convergence rate. This iterative process continues until the objective function $J(\boldsymbol{\theta})$ is minimized, resulting in an optimal control sequence that prepares the desired quantum state with high fidelity.

3) DQL: Deep RL (DRL) combines RL with DL to optimize control strategies for manipulating quantum systems. The environment simulates the quantum dynamics, including methods to reset the system, apply control actions, and compute rewards. A quantum state is input to the deep Q-network, which approximates the Q-function, estimating the expected cumulative reward for each state-action pair. Actions adjust the control function $\epsilon(t)$, while the reward, based on infidelity as given in (12), encourages the agent to minimize the error, offering higher rewards as the state approaches the target. The DQL leverages the Bellman equation to iteratively update the Q-function, which estimates the optimal action-value function. The Q-function is approximated using a neural network consisting of two key networks: *evaluation* and *target* networks. The evaluation network is trained to predict Q-values, while the target network provides stable targets for training. The training process involves storing state, action, and reward experiences in a replay buffer, sampling batches of these experiences, and updating the evaluation network by minimizing the loss between the predicted Q-values and the target Q-values. Periodically, the target network is updated to match the evaluation network, ensuring stability during training. The agent employs a q-greedy strategy to balance exploration and exploitation: it explores by choosing a random action with probability q, and exploits by selecting the best-known action of the highest Q-value with probability $1-q$. The goal is to maximize cumulative reward, which is linked to achieving high fidelity between the quantum state and the target state, as measured by the final overlap after training.

C. Numerical Examples

We present a numerical example for image-based anomaly (defect) detection in industrial CPS networks. A ML algorithm extracts an anomaly semantic map from images, which is then segmented and converted into hull point data $\mathcal{P}$. This data is then transmitted using quantum communication with quantum states prepared by quantum optimal pulse control. At the receiver end, quantum optimal decision-making is used to decode the data and reconstruct the hull point information. This anomaly map is then overlaid onto a template image to provide a semantic understanding of the defect location, facilitating easier quality control and relevant corrective actions.

1) ML Model and Dataset: Anomalib [75], a deep-learning library for anomaly detection, is used to train the FastFlow model on the MVTec AD dataset for each specific case. The dataset contains over $5,000$ high-resolution images across 15 different categories, including objects like bottles, cables, and wood. Each category includes both defect-free images and images with various types of defects, along with detailed pixel-level annotations for the defective regions. The MVTec AD dataset is widely used to develop and benchmark algorithms for detecting and localizing anomalies in industrial settings, making it a crucial resource in the field of machine vision and quality control.

Specifically, we utilize the ResNet-18 backbone and 8 flow steps. Each category in the dataset is trained separately using a batch size of 32. The optimizer used to train the FastFlow model for anomaly detection is designed to maximize the area under the receiver operating characteristic curve. This metric, ranging from 0 to 1, measures the model ability to differentiate between normal and anomalous samples, with higher values indicating better performance.

2) BPSK QSC with Qubit Control: For DV qubit control, we consider a qubit on a two-level quantum system. The drift Hamiltonian $\boldsymbol{\mathcal{H}}_{\mathrm{d}}$ is given by

$$\boldsymbol{\mathcal{H}}_{\mathrm{d}} = -\frac{\omega}{2}\boldsymbol{\sigma}_{\mathrm{x}} \tag{14}$$

where ω denotes the energy separation between the qubit levels and $\boldsymbol{\sigma}_{\mathrm{x}} = |0\rangle\langle 1| + |1\rangle\langle 0|$ is the Pauli-x operator. The control Hamiltonian $\boldsymbol{\mathcal{H}}_{\mathrm{c}}$ is given by

$$\boldsymbol{\mathcal{H}}_{\mathrm{c}} = \epsilon(t)\,\gamma\boldsymbol{\sigma}_{\mathrm{z}} \tag{15}$$

where γ is a constant coefficient and $\boldsymbol{\sigma}_{\mathrm{z}} = |0\rangle\langle 0| - |1\rangle\langle 1|$ is the Pauli-z operator. The control function $\epsilon(t)$ drives transitions between the qubit states. For simplicity, we use a sequence

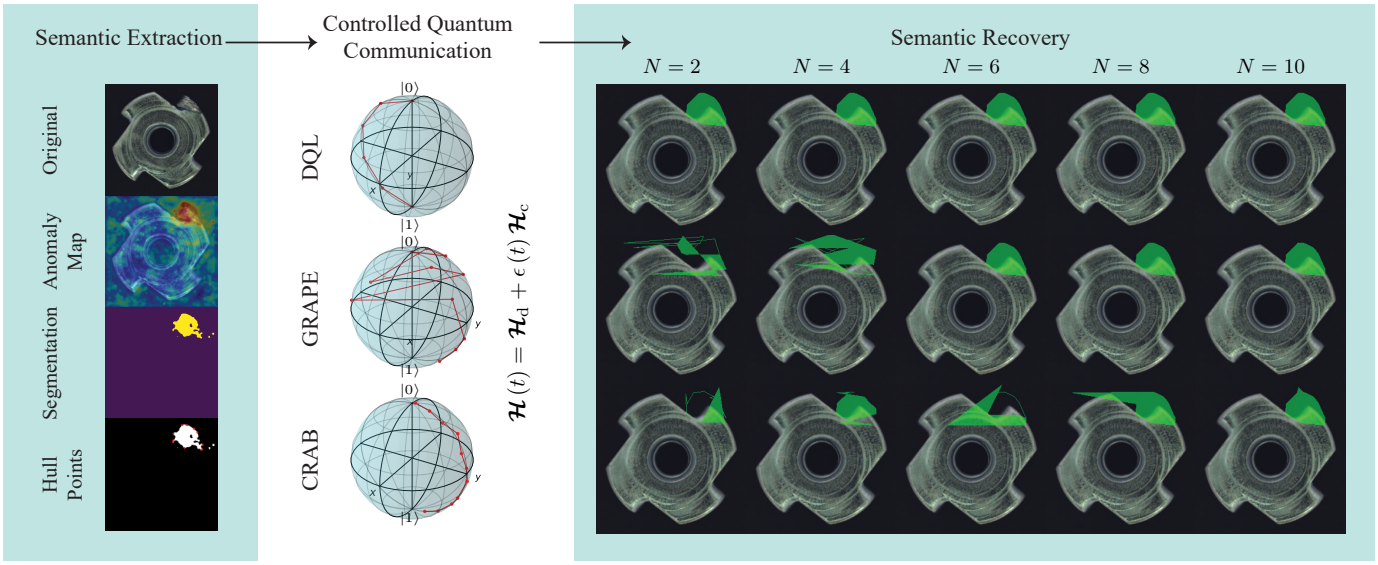

Fig. 6. Defect detection for a metal nut with controlled BPSK QSC. The left panel demonstrates the semantic extraction process, including the original image, anomaly map, and segmentation to identify defects, followed by extracting hull point vectors. The middle panel showcases the controlled qubit state preparation for quantum communication using DQL, GRAPE, and CRAB QOC to transmit the semantic information securely with high fidelity. The right panel illustrates the recovery of the semantic information at different quantization levels N of control.

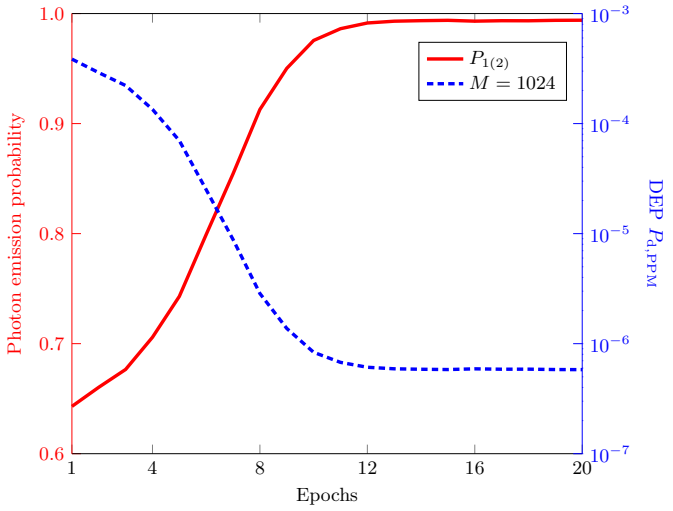

Fig. 7. The controlled photon emission probability $P_{1(2)}$ and DEP $P_{\mathrm{d,PPM}}$ for 1024-PPM QSC with the Gaussian pulse control as a function of epochs for the differential evolution Nelder–Mead algorithm.

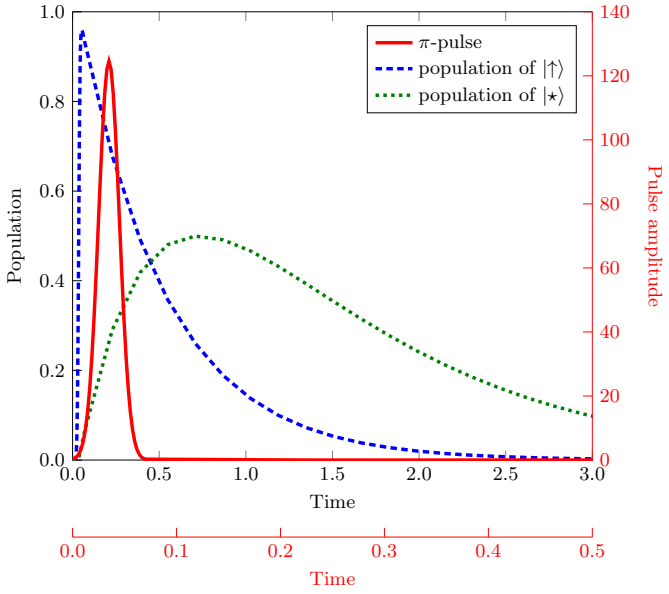

Fig. 8. Dynamics of the optimized π-pulse and populations (system expectation values) $\langle \mathbf{\Pi}_{\uparrow} \rangle$ and $\langle \mathbf{\Pi}_{\star} \rangle$ of the excited state $|\uparrow\rangle$ and the intermediate state $|\star\rangle$, where the system decays from the excited state.

of piecewise constant pulses, each with an identical duration. The total time $T = 2\pi$ is split into N time intervals or control intervals, with each piece having a duration of $\Delta t = T/N$. The total evolution time may be shorter than T, depending on the algorithm's efficiency. The control function $\epsilon(t)$ is discretized for each interval. In numerical examples, we set the main parameters as $\omega = 1$, $\gamma = 4$, $K = 5$ for CRAB, $\delta = 0.01$ for GRAPE, and $q = 0.9$ for DQL.

Fig. 3 shows controlled pulse amplitudes, quantum state fidelity, and DEP $P_{\mathrm{d,BPSK}}$ for BPSK QSC with DQL, GRAPE, and CRAB qubit control. For quantum state preparation starting from $|\psi_0\rangle$ to $|\psi_1\rangle$, the controlled pulse amplitudes are plotted for 10 time intervals ($N = 10$) at each time step in T (left). Averaging over $20,000$ runs, quantum state fidelity $\left|\langle\psi_1|\hat{\psi}_1\rangle\right|^2$ and $P_{\mathrm{d,BPSK}}$ are also depicted as a function of time intervals N for three QOC algorithms (right). It can be observed that DQL achieves the most effective (near-ideal) qubit control within lesser time steps as shown in Fig. 3. This is attributed to the DQL agent's ability to rapidly learn and explore the control space. At each control interval within T for DQL, GRAPE, and CRAB qubit control, when $N = 10$, the Wigner function [76] of state evolution from $|\psi_0\rangle$ to $|\psi_1\rangle$ is shown in Fig. 4. The figure illustrates the evolution of the Wigner function in phase space across successive time steps.

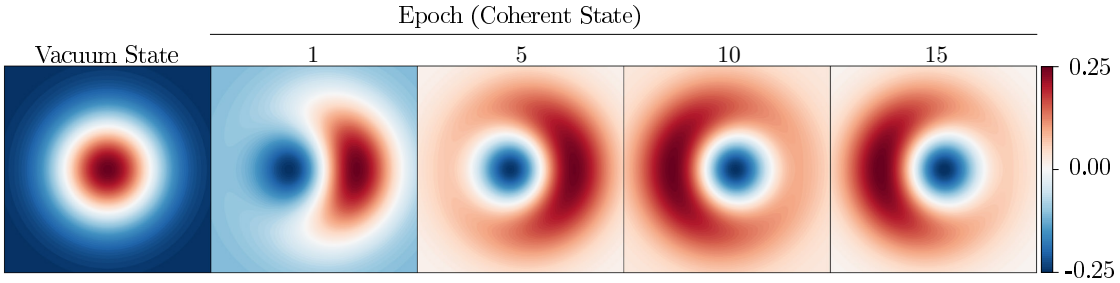

Fig. 9. Wigner function of the controlled coherent state $|\eta\rangle$ by optimization with the evolution from the vacuum state to progressively optimized coherent states over the course of epochs.

In each plot, the horizontal and vertical axes represent the amplitude (real part) and phase quadratures (imaginary part), respectively. Positive (red) and negative (blue) regions reveal the quasi-probability distribution. These plots demonstrate the progression of the quantum state under QOC, capturing the quantum dynamics induced by the applied control.

To further ascertain the BPSK QSC performance in transmitting the hull point vector of defected regions, Fig. 5 shows the mean intersection over union (mIoU) [77], the normalized mean squared error (NMSE), the structural similarity index measure (SSIM) [78], and the Hausdorff distance [79] for anomaly detection as a function of time intervals N for BPSK QSC with DQL, GRAPE, and CRAB qubit control. These metrics are averaged across all categories in the MVTec AD dataset and their respective defects. The mIoU measures the overlap between the predicted and actual semantic regions, indicating how accurately the transmitted content reflects the original semantic categories. The NMSE evaluates the overall fidelity of the transmitted signal by quantifying the squared error between the original and transmitted content, with lower values indicating higher accuracy. The SSIM assesses how well the structural information of the data, such as textures and edges, is preserved, which is vital for retaining the perceived meaning. Finally, the Hausdorff distance measures the maximum deviation between the spatial arrangements of semantic elements in the predicted and ground-truth data, ensuring that the transmitted shapes and boundaries remain intact. Fig. 5 demonstrates again the DQL maintains near-ideal control even at lower time intervals, indicating its robustness and efficiency in dealing with the inherent complexities of quantum system dynamics. In Fig. 6, we show an example of metal nut anomaly detection. These examples also suggest that while GRAPE and CRAB can be effective under certain conditions, their control performances are more sensitive to the complexity of control landscapes, requiring further optimization for emerging quantum communication applications.

V. Controlled CV QSC for Anomaly Detection

Reliable generation of photons is essential for CV quantum states. In this section, we provide a controlled CV QSC system for industrial anomaly detection using quantum M-PPM where optimal pulse control manipulates a quantum dot system for a photon source. This QOC enables the generation of photons for coherent quantum states that are subsequently utilized in the M-PPM QSC framework.

A. Quantum M-PPM

Quantum M-PPM is one of the most robust quantum communication modulations. This modulation encodes information in the presence or absence of a coherent state $|\eta\rangle$ in a particular time slot. The quantum state for the mth symbol is given by

$$|\psi_m\rangle = |0\rangle_1 \otimes |0\rangle_2 \otimes \cdots \otimes |\eta\rangle_m \otimes \cdots \otimes |0\rangle_M \tag{16}$$

where $m = 1, 2, \ldots, M$, $|\eta\rangle_m$ represents the coherent state in the mth time slot, and $|0\rangle_k$ denotes the vacuum state (i.e., no photon) in the kth time slot for $k \neq m$. The coherent state $|\eta\rangle$ can be written as [33]

$$|\eta\rangle = e^{-|\eta|^2/2} \sum_{\ell=0}^{\infty} \frac{\eta^\ell}{\sqrt{\ell!}} |\ell\rangle \tag{17}$$

where $|\ell\rangle$ is the Fock (number) state with exactly ℓ photons and η is a complex number related to the average photon number $|\eta|^2$. Since the M-PPM states have the geometrically uniform symmetry, the square-root measurement produces an optimal decision, leading to DEP for quantum M-PPM as follows [33]:

$$P_{\mathrm{d,PPM}} = 1 - \frac{1}{M^2}\left(\sqrt{1+(M-1)\,\zeta} + (M-1)\sqrt{1-\zeta}\right)^2 \tag{18}$$

where $\zeta = \mathrm{e}^{-2|\eta|^2 \log_2 M}$ is the superposition degree.

B. Controlled CV Quantum State Preparation

Quantum dots are semiconductor nanocrystals that confine electrons in all three spatial dimensions, resulting in discrete energy levels similar to those of atoms. They are excellent sources of single photons due to their ability to emit photons one at a time upon excitation [80]. Using quantum dots as photon emitters in quantum M-PPM communication enables secure and efficient information transmission by leveraging the quantum property of light. We consider the dynamics of a biexcitonic system in a quantum dot—i.e., a three-level quantum system that emits two photons through a cascaded decay process [41]. The three-level system consists of the ground state $|\downarrow\rangle$, the intermediate state $|\star\rangle$, and the excited state $|\uparrow\rangle$. The system Hamiltonian consists of time-independent and time-dependent (interaction Hamiltonian) parts. The total Hamiltonian can be written as [41]

$$\boldsymbol{\mathcal{H}}(t) = \frac{\mathcal{E}}{2}|\star\rangle\langle\star| + \boldsymbol{\mathcal{H}}_\star(t) \tag{19}$$

where the first term represents the unperturbed energy of the system associated with the intermediate state $|\star\rangle$, $\mathcal{E}$ denotes the binding energy, and $\boldsymbol{\mathcal{H}}_\star(t)$ describes the interaction between the quantum system and the driving electric field in the rotating wave approximation. The interaction Hamiltonian $\boldsymbol{\mathcal{H}}_\star(t)$ is given by

$$\boldsymbol{\mathcal{H}}_\star(t) = \frac{\mu\,\epsilon^2(t)}{\mathcal{E}}\left(|\downarrow\rangle\langle\uparrow| + |\uparrow\rangle\langle\downarrow|\right) \tag{20}$$

where μ is the coupling strength of the system to the field and $\epsilon(t)$ is the time-dependent electric field driving the excitation process. The decay from $|\uparrow(\star)\rangle$ to $|\star(\downarrow)\rangle$ while emitting the first (second) photon is given by a collapse operator as follows [81]:

$$\boldsymbol{\sigma}_{1(2)} = \sqrt{\gamma_{1(2)}}\;|\star(\downarrow)\rangle\langle\uparrow(\star)| \tag{21}$$

where the parameter $\gamma_{1(2)}$ denotes the decay rate for the first (second) channel.

The system evolution is governed by the Lindblad master equation, which describes both coherent evolution due to the Hamiltonian and incoherent decay processes as follows [41], [82]:

$$\frac{\partial\boldsymbol{\rho}}{\partial t} = \mathcal{L}\boldsymbol{\rho} = -\imath\left[\boldsymbol{\mathcal{H}}_\star(t), \boldsymbol{\rho}\right] + \sum_{k=1}^{2}\mathcal{D}\left[\boldsymbol{\sigma}_k\right]\boldsymbol{\rho} \tag{22}$$

where $\mathcal{L}$ is the Liouvillian superoperator that describes the system time evolution and $\mathcal{D}$ is the Lindblad dissipator accounting for the system coupling to its environment. The dissipative dynamics of the system, which account for photon emissions into the decay channels, are represented by the terms

$$\mathcal{D}\left[\boldsymbol{\sigma}_k\right]\boldsymbol{\rho} = \boldsymbol{\sigma}_k\boldsymbol{\rho}\boldsymbol{\sigma}_k^\dagger - \frac{1}{2}\left(\boldsymbol{\sigma}_k^\dagger\boldsymbol{\sigma}_k\boldsymbol{\rho} + \boldsymbol{\rho}\boldsymbol{\sigma}_k^\dagger\boldsymbol{\sigma}_k\right) \tag{23}$$

where $\dagger$ denotes the conjugate transpose. Note that the system starts in the ground state $|\downarrow\rangle$ and evolves according to the master equation. The populations of the excited state $|\uparrow\rangle$ and the intermediate state $|\star\rangle$ can be tracked over time using the projection operators as follows:

$$\langle\boldsymbol{\Pi}_\uparrow\rangle = \langle\uparrow|\,\boldsymbol{\rho}\,|\uparrow\rangle \tag{24}$$

$$\langle\boldsymbol{\Pi}_\star\rangle = \langle\star|\,\boldsymbol{\rho}\,|\star\rangle, \tag{25}$$

respectively. The number of photons emitted into the first and second channels is always equal due to the cascaded nature of the system. We can choose to monitor (condition) the emission from either channel while tracing over the state of only one channel.

Let $P_{1(2)}$ be the probability of a single-photon emission into the first (second) channel. Since the system can emit only one photon per channel, this emission probability is equal to the average number of photons emitted into each channel. Using the formalism of conditioned evolution [41], [83], we obtain

$$P_{1(2)} = \int_0^\infty \mathrm{tr}\Big[\mathcal{K}_{1(2)}(t,\infty)\,\boldsymbol{\sigma}_{1(2)}\left(\mathcal{K}_{1(2)}(0,t)\,|\downarrow\rangle\langle\downarrow|\right)\boldsymbol{\sigma}_{1(2)}^\dagger\Big]dt \tag{26}$$

where $\mathrm{tr}(\cdot)$ denotes the trace operator and the superoperator $\mathcal{K}_{1(2)}(t_1,t_2)$ represents the nonunitary evolution of the quantum system conditioned on no photon emission during a time interval from t_1 to t_2, defined by the relationship

$$\mathcal{K}_{1(2)}\boldsymbol{\rho} = \mathcal{L}\boldsymbol{\rho} - \boldsymbol{\sigma}_{1(2)}\boldsymbol{\rho}\boldsymbol{\sigma}_{1(2)}^\dagger. \tag{27}$$

The control problem here is to optimize the pulse $\epsilon(t)$ to maximize the photon emission probability $P_{1(2)}$ or equivalently, the average photon number. Specifically, the aim is to ensure that each channel emits exactly one photon with high probability. These photons will then be used to generate coherent states for quantum M-PPM communication.

C. Numerical Examples

We consider the ML model and the dataset in Section IV-C again. To control the quantum system, the pulse $\epsilon(t)$ in (20) plays a crucial role in driving transitions between quantum states to generate photons. Herein, we model the π-pulse using a Gaussian pulse, controlled by parameters such as the pulse width and offset as follows:

$$\epsilon(t) = \frac{1}{\sqrt{2\pi\chi^2}}\exp\left[-\frac{(t-t_0)^2}{2\chi^2}\right] \tag{28}$$

where χ controls the pulse width and t_0 is the time offset (the pulse center). In numerical examples, we set $t_0 = 3$ and $2\gamma_2 = \gamma_1 = \mathcal{E} = \mu = 1$. The objective is to optimize the pulse width to maximize the probability of emitting a single photon into either channel. This optimization makes the system behave as a two-photon source, as the photons are emitted in a cascaded manner such that the average photon number is equal to $|\eta|^2 = P_1 + P_2$. In this system, we only need to optimize the pulse for the average number of photons emitted into the first (or second) channel, i.e., P_1 (or P_2), as the optimized pulse produces the second (or first) photon with the same expectation value. To optimize the pulse width (i.e., χ) for maximizing the photon emission probability $P_{1(2)}$, we use the Nelder–Mead algorithm [84], with bounds set to $(0.002, 2)$.

Fig. 7 shows the convergence of the differential evolution (Nelder–Mead) algorithm for the Gaussian pulse control to maximize the photon emission probability $P_{1(2)}$, averaging over $1,000$ runs. The DEP $P_{\mathrm{d,PPM}}$ for quantum M-PPM is also depicted when $M = 2^{10}$. The algorithm converges with the optimal χ of 0.01, maximizing the photon emission probability (i.e., the average photon number per channel) close to unity. The corresponding coherent state $|\eta\rangle$ has the average photon number of $|\eta|^2 = 1.98$, indicating that the system will likely emit two photons with high probability. Using this controlled coherent state, we achieve a decent $P_{\mathrm{d,PPM}}$ of 5.917×10^{-7} for the quantum 1024-PPM, suitable for reliable industrial CPS communication. The π-pulse shape and system dynamics are shown in Fig. 8. The excited state $|\uparrow\rangle$ decays twice as fast as the intermediate state $|\star\rangle$. Fig. 9 illustrates the resulting coherent state evolution by optimization in the Wigner function plot.

We simulate the controlled M-PPM QSC system for transmitting data of defected regions using the optimized coherent states, where the receiver again reconstructs the hull point data $\mathcal{P}$ and overlays it on a template image as in BPSK QSC, over multiple runs. The defect detection results for four (capsule, bottle, carpet, and metal nut) classes are shown in Fig. 10 when $M = 1024$. In this example, we get the mIoU score of 0.999, indicating substantial segmentation accuracy across all defect classes in the MVTec AD dataset. The SSIM

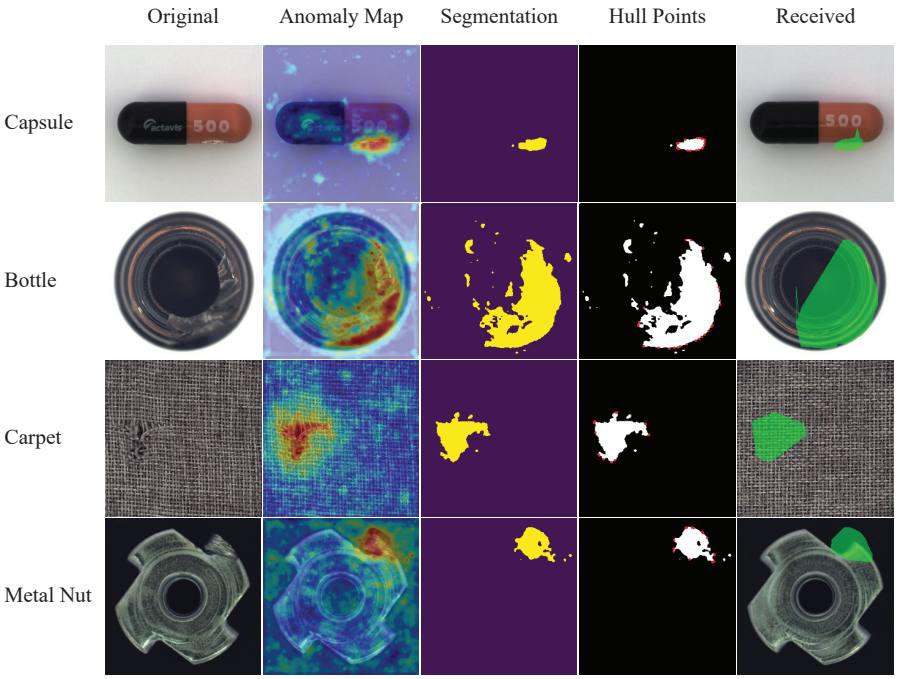

Fig. 10. Defect detection for four (capsule, bottle, carpet, and metal nut) classes with controlled 1024-PPM QSC.

score of 0.999 again highlights the ability to maintain high structural similarity between the predicted and ground-truth images. A very low NMSE of 5.26×10^{-6} suggests minimal reconstruction error, while the Hausdorff distance of 0.0011 reflects robust performance for industrial applications. All these metrics demonstrate that the controlled QSC framework performs reliably across diverse defect classes, achieving effective segmentation with minimal structural deviations.

VI. Conclusion

Industrial IoT and CPS networks face significant challenges, particularly in data security and communication efficiency. Semantic communication presents a promising computing-intensive solution by transmitting only the essential meaning of the data. In this paper, we have developed the integrated QSC framework with QOC. Specifically, for the task of anomaly detection in industrial environments, we have employed the DL algorithm to extract semantic hull points from images of defective products. These points are transmitted using secure quantum BPSK and M-PPM communication. To prepare the required DV and CV quantum states, we have utilized pulse control of quantum systems, enabling high-fidelity transmission of the hull points. The receiver reconstructs these points as anomaly maps, effectively retrieving the semantic information of the anomaly regions. This approach offers a secure and controlled method for communicating critical data in industrial CPS networks.

References

[1] A. Colombo, S. Karnouskos, Y. Shi, and S. Yin, "Industrial cyber-physical systems: A backbone of the fourth industrial revolution," *IEEE Ind. Electron. Mag.*, vol. 11, no. 1, pp. 6–16, Mar. 2017.

[2] F. Tao, H. Zhang, and A. Liu, "Digital twins and cyber-physical systems toward smart manufacturing and Industry 4.0," *IEEE Trans. Ind. Informat.*, vol. 15, no. 4, pp. 2405–2415, Apr. 2019.

[3] B. Chen, J. Wan, L. Shu, P. Li, M. Mukherjee, and B. Yin, "Smart factory of Industry 4.0: Key technologies, application case, and challenges," *IEEE Access*, vol. 6, pp. 6505–6519, Dec. 2017.

[4] A. Mostaani, T. X. Vu, S. K. Sharma, V.-D. Nguyen, Q. Liao, and S. Chatzinotas, "Task-oriented communication design in cyber-physical systems: A survey on theory and applications," *IEEE Access*, vol. 10, pp. 133 842–133 868, Dec. 2022.

[5] L. Li, K. Ota, and M. Dong, "Deep learning for smart Industry: Efficient manufacture inspection system with fog computing," *IEEE Trans. Ind. Informat.*, vol. 14, no. 10, pp. 4665–4673, Oct. 2018.

[6] J. Wan, J. Yang, Z. Wang, and Q. Hua, "Artificial intelligence for cloud-assisted smart factory," *IEEE Access*, vol. 6, pp. 55 419–55 430, Sep. 2018.

[7] J. Wang, L. Wu, K.-K. R. Choo, and D. He, "Blockchain-based anonymous authentication with key management for smart grid edge computing infrastructure," *IEEE Trans. Ind. Informat.*, vol. 16, no. 3, pp. 1984–1992, Mar. 2020.

[8] J. Wan, S. Tang, H. Yan, D. Li, and S. Wang, "Software-defined industrial Internet of Things in the context of Industry 4.0," *IEEE Sensors J.*, vol. 16, no. 20, pp. 7373–7380, Oct. 2016.

[9] A. M. Ramly, N. F. Abdullah, and R. Nordin, "Cross-layer design and performance analysis for ultra-reliable factory of the future based on 5G mobile networks," *IEEE Access*, vol. 9, p. 68161–68175, May 2021.

[10] Y. Yang, C. Guo, F. Liu, C. Liu, L. Sun, Q. Sun, and J. Chen, "Semantic communications with artificial intelligence tasks: Reducing bandwidth requirements and improving artificial intelligence task performance," *IEEE Ind. Electron. Mag.*, pp. 2–11, May 2022.

[11] U. Khalid, M. S. Ulum, A. Farooq, T. Q. Duong, O. A. Dobre, and H. Shin, "Quantum semantic communications for Metaverse: Principles and challenges," *IEEE Wireless Commun.*, vol. 30, no. 4, pp. 26–36, Aug. 2023.

[12] H. Xie and Z. Qin, "A lite distributed semantic communication system for Internet of Things," *IEEE J. Sel. Areas Commun.*, vol. 39, no. 1, pp. 142–153, Jan. 2021.

[13] S. Tariq, U. Khalid, B. E. Arfeto, T. Q. Duong, and H. Shin, "Integrating sustainable big AI: Quantum anonymous semantic broadcast," *IEEE Wireless Commun.*, vol. 31, no. 3, pp. 86–99, Jun. 2024.

[14] F. Zaman, A. Farooq, M. A. Ullah, H. Jung, H. Shin, and M. Z.

Win, "Quantum machine intelligence for 6G URLLC," *IEEE Wireless Commun.*, vol. 30, no. 2, pp. 22–30, Apr. 2023.

[15] U. Khalid, J. ur Rehman, S. N. Paing, H. Jung, T. Q. Duong, and H. Shin, "Quantum network engineering in the NISQ age: Principles, missions, and challenges," *IEEE Netw.*, vol. 38, no. 1, pp. 112–123, Jan. 2024.

[16] G. Rathee, A. Sharma, R. Kumar, and R. Iqbal, "A secure communicating things network framework for industrial IoT using blockchain technology," *Ad Hoc Netw.*, vol. 94, p. 101933, Nov. 2019.

[17] M. R. Asghar, Q. Hu, and S. Zeadally, "Cybersecurity in industrial control systems: Issues, technologies, and challenges," *Comput. Netw.*, vol. 165, p. 106946, Dec. 2019.

[18] H. Kayan, M. Nunes, O. Rana, P. Burnap, and C. Perera, "Cybersecurity of industrial cyber-physical systems: A review," *ACM Comput. Surv.*, vol. 54, no. 11s, pp. 1–35, Sep. 2022.

[19] J. Biamonte, P. Wittek, N. Pancotti, P. Rebentrost, N. Wiebe, and S. Lloyd, "Quantum machine learning," *Nature*, vol. 549, no. 7671, pp. 195–202, Sep. 2017.

[20] S. Tariq, B. E. Arfeto, U. Khalid, S. Kim, T. Q. Duong, and H. Shin, "Deep quantum-transformer networks for multimodal beam prediction in ISAC systems," *IEEE Internet Things J.*, vol. 11, no. 18, pp. 29 387–29 401, Sep. 2024.

[21] A. Bayerstadler, G. Becquin, J. Binder, T. Botter, and et al., "Industry quantum computing applications," *EPJ Quantum Technol.*, vol. 8, no. 1, p. 25, Nov. 2021.

[22] A. Perdomo-Ortiz, A. Feldman, A. Ozaeta, and et al., "Readiness of quantum optimization machines for industrial applications," *Phys. Rev. A*, vol. 12, no. 1, p. 014004, Jul. 2019.

[23] M. S. Ulum, U. Khalid, J. W. Setiawan, T. Q. Duong, M. Z. Win, and H. Shin, "Variational anonymous quantum sensing," *IEEE J. Sel. Areas Commun.*, vol. 42, no. 9, pp. 2275–2291, Sep. 2024.

[24] S. N. Paing, J. W. Setiawan, M. A. Ullah, F. Zaman, T. Q. Duong, O. A. Dobre, and H. Shin, "Counterfactual quantum Byzantine consensus for human-centric Metaverse," *IEEE J. Sel. Areas Commun.*, vol. 42, no. 4, pp. 905–918, Apr. 2024.

[25] N. Gisin and R. Thew, "Quantum communication," *Nat. Photonics*, vol. 1, no. 3, pp. 165–171, Mar. 2007.

[26] D. Cozzolino, B. D. Lio, D. Bacco, and L. K. Oxenløwe, "High-dimensional quantum communication: Benefits, progress, and future challenges," *Adv. Quantum Technol.*, vol. 2, no. 12, p. 1900038, Oct. 2019.

[27] S. N. Paing, J. W. Setiawan, T. Q. Duong, D. Niyato, M. Z. Win, and H. Shin, "Quantum anonymous networking: A quantum leap in privacy," *IEEE Netw.*, vol. 38, no. 5, pp. 131–145, Sep. 2024.

[28] M. M. Wilde, *Quantum Information Theory*, 2nd ed. Cambridge, U.K.: Cambridge Univ. Press, 2017.

[29] F. Zaman, S. N. Paing, A. Farooq, H. Shin, and M. Z. Win, "Concealed quantum telecomputation for anonymous 6G URLLC networks," *IEEE J. Sel. Areas Commun.*, vol. 41, no. 7, pp. 2278–2296, Jul. 2023.

[30] W. Yang, H. Du, Z. Liew, W. Y. B. Lim, Z. Xiong, D. Niyato, X. Chi, X. S. Shen, and C. Miao, "Semantic communications for future internet: Fundamentals, applications, and challenges," *IEEE Commun. Surveys Tuts.*, vol. 25, no. 1, pp. 213–250, Nov. 2023.

[31] F. Zaman, U. Khalid, T. Q. Duong, H. Shin, and M. Z. Win, "Quantum full-duplex communication," *IEEE J. Sel. Areas Commun.*, vol. 41, no. 9, pp. 2966–2980, Sep. 2023.

[32] L. Oleynik, J. U. Rehman, H. Al-Hraishawi, and S. Chatzinotas, "Variational estimation of optimal signal states for quantum channels," *IEEE Trans. Quantum Eng.*, vol. 5, pp. 1–8, Apr. 2024.

[33] G. Cariolaro, *Quantum Communications*, 1st ed. Cham, Switzerland.: Springer, 2015.

[34] C. W. Helstrom, "Quantum detection and estimation theory," *J. Stat. Phys.*, vol. 1, pp. 231–252, 1969.

[35] J. Yu, Y. Zheng, X. Wang, W. Li, Y. Wu, R. Zhao, and L. Wu, "Fastflow: Unsupervised anomaly detection and localization via 2D normalizing flows," *arXiv:2111.07677*, Nov. 2021.

[36] T. Caneva, T. Calarco, and S. Montangero, "Chopped random-basis quantum optimization," *Phys. Rev. A*, vol. 84, no. 2, p. 022326, Aug. 2011.

[37] P. de Fouquieres, S. G. Schirmer, S. J. Glaser, and I. Kuprov, "Second order gradient ascent pulse engineering," *J. Magn. Reson.*, vol. 212, no. 2, pp. 412–417, Aug. 2011.

[38] G. Jäger, D. M. Reich, M. H. Goerz, C. P. Koch, and U. Hohenester, "Optimal quantum control of Bose-Einstein condensates in magnetic microtraps: Comparison of gradient-ascent-pulse-engineering and Krotov optimization schemes," *Phys. Rev. A*, vol. 90, no. 3, p. 033628, Sep. 2014.

[39] M. Bukov, A. G. R. Day, D. Sels, P. Weinberg, A. Polkovnikov, and P. Mehta, "Reinforcement learning in different phases of quantum control," *Phys. Rev. X*, vol. 8, no. 3, p. 031086, Sep. 2018.

[40] M. Y. Niu, S. Boixo, V. N. Smelyanskiy, and H. Neven, "Universal quantum control through deep reinforcement learning," *npj Quantum Inform.*, vol. 5, no. 1, p. 33, Apr. 2019.

[41] L. Hanschke, K. A. Fischer, S. Appel, and et al., "Quantum dot single-photon sources with ultra-low multi-photon probability," *npj Quantum Inform.*, vol. 4, p. 43, Sep. 2018.

[42] C. E. Shannon, "A mathematical theory of communication," *BSTJ*, vol. 27, pp. 623–656, Jul. 1948.

[43] M. A. Nielsen and I. L. Chuang, *Quantum Computation and Quantum Information*. Cambridge, UK: Cambridge University Press, 2000.

[44] V. Scarani, H. Bechmann-Pasquinucci, N. J. Cerf, M. Dušek, N. Lütkenhaus, and M. Peev, "The security of practical quantum key distribution," *Rev. Mod. Phys.*, vol. 81, no. 3, pp. 1301–1350, Sep 2009.

[45] A. Unnikrishnan, I. J. MacFarlane, R. Yi, E. Diamanti, D. Markham, and I. Kerenidis, "Anonymity for practical quantum networks," *Phys. Rev. Lett.*, vol. 122, no. 24, p. 240501, Jun. 2019.

[46] M. Chehimi, C. Chaccour, and W. Saad, "Quantum semantic communications: An unexplored avenue for contextual networking," *arXiv:2205.02422*, May 2022.

[47] M. Chehimi, C. Chaccour, C. K. Thomas, and W. Saad, "Quantum semantic communications for resource-efficient quantum networking," *IEEE Wireless Commun. Lett.*, vol. 28, no. 4, pp. 803–807, Apr. 2024.

[48] N. Nunavath, E. C. Strinati, R. Bassoli, and F. H. P. Fitzek, "Pragmatic semantic communication through quantum channel," in *Proc. IEEE 3rd Int. Conf. 6G Networking (6GNet)*, Oct. 2024, pp. 189–195.

[49] U. Khalid, M. S. Ulum, A. Farooq, T. Q. Duong, O. A. Dobre, and H. Shin, "Quantum semantic communications for Metaverse: Principles and challenges," *IEEE Wireless Commun.*, vol. 30, no. 4, pp. 26–33, 2023.

[50] J. Preskill, "Quantum computing in the NISQ era and beyond," *Quantum*, vol. 2, p. 79, Aug. 2018.

[51] Z.-Q. Zhao, P. Zheng, S.-T. Xu, and X. Wu, "Object detection with deep learning: A review," *IEEE Trans. Neural Netw. Learn. Syst.*, vol. 30, no. 11, pp. 3212–3232, Nov. 2019.

[52] K. Imoto, T. Nakai, T. Ike, K. Haruki, and Y. Sato, "A CNN-based transfer learning method for defect classification in semiconductor manufacturing," *IEEE Trans. Semicond. Manuf.*, vol. 32, no. 4, pp. 455–459, Apr. 2019.

[53] Z. Huang, J. Zhu, J. Lei, X. Li, and F. Tian, "Tool wear predicting based on multi-domain feature fusion by deep convolutional neural network in milling operations," *J. Intell. Manuf.*, vol. 31, no. 4, pp. 953–966, 2020.

[54] H. Huang *et al.*, "Real-time fault detection for IIoT facilities using GBRBM-based DNN," *IEEE Internet Things J.*, vol. 7, no. 7, pp. 5713–5722, Jul. 2020.

[55] Y. Huang, J. Jing, and Z. Wang, "Fabric defect segmentation method based on deep learning," *IEEE Trans. Instrum. Meas.*, vol. 70, pp. 1–15, Jan. 2021.

[56] T. Wang, Y. Yao, Y. Chen, M. Zhang, F. Tao, and H. Snoussi, "Auto-sorting system toward smart factory based on deep learning for image segmentation," *IEEE Sensors J.*, vol. 18, no. 20, pp. 8493–8501, Oct. 2018.

[57] M. Ghahramani, Y. Qiao, M. Zhou, A. O'Hagan, and J. Sweeney, "AI-based modeling and data-driven evaluation for smart manufacturing processes," *IEEE/CAA J. Autom. Sinica*, vol. 7, no. 4, pp. 1026–1037, Jul. 2020.

[58] C. Dai, X. Liu, H. Xu, L. T. Yang, and J. Deen, "Hybrid deep model for human behavior understanding on industrial Internet of Video Things," *IEEE Trans. Ind. Informat.*, vol. 18, no. 10, pp. 7000–7008, Oct. 2022.

[59] M. de Berg, M. van Kreveld, M. Overmars, and O. Schwarzkopf, *Computational Geometry: Algorithms and Applications*, 2nd ed. Berlin, Germany: Springer, 2000.

[60] C. H. Bennett and G. Brassard, "Quantum cryptography: Public key distribution and coin tossing," *Theor. Comput. Sci.*, vol. 560, pp. 7–11, Dec. 2014.

[61] W. K. Wootters and W. H. Zurek, "A single quantum cannot be cloned," *Nature*, vol. 299, no. 5886, pp. 802–803, Oct 1982.

[62] V. Lipinska, G. Murta, and S. Wehner, "Anonymous transmission in a noisy quantum network using the W state," *Phys. Rev. A*, vol. 98, no. 5, p. 052320, Nov. 2018.

[63] W. Yang, L. Huang, and F. Song, "Privacy preserving quantum anonymous transmission via entanglement relay," *Sci. Rep.*, vol. 6, no. 1, p. 26762, Jun. 2016.

[64] A. Khan, U. Khalid, J. ur Rehman, and H. Shin, "Quantum anonymous private information retrieval for distributed networks," *IEEE Trans. Commun.*, vol. 70, no. 6, pp. 4026–4037, Apr. 2022.
[65] R.-h. Shi and X.-q. Fang, "Anonymous classical message transmission through various quantum networks," *IEEE Trans. Netw. Sci. Eng.*, vol. 11, no. 3, pp. 2901–2913, May 2024.
[66] R. Kaewpuang, M. Xu, W. Y. B. Lim, D. Niyato, H. Yu, J. Kang, and X. Shen, "Cooperative resource management in quantum key distribution QKD networks for semantic communication," *IEEE Internet Things J.*, vol. 11, no. 5, pp. 4454–4469, Feb. 2023.
[67] D. Bouwmeester, J.-W. Pan, K. Mattle, M. Eibl, H. Weinfurter, and A. Zeilinger, "Experimental quantum teleportation," *Nature*, vol. 390, pp. 575–579, Dec. 1997.
[68] S. Olmschenk, D. N. Matsukevich, P. Maunz, D. Hayes, L. Duan, and C. Monroe, "Quantum teleportation between distant matter qubits," *Science*, vol. 323, pp. 486–489, Jan. 2009.
[69] A. Furusawa, J. L. Sørensen, S. L. Braunstein, C. A. Fuchs, H. J. Kimble, and E. S. Polzik, "Unconditional quantum teleportation," *Science*, vol. 282, pp. 706–709, Oct. 1998.
[70] F. Grosshans and P. Grangier, "Continuous variable quantum cryptography using coherent states," *Phys. Rev. Lett.*, vol. 88, no. 5, p. 057902, Jan. 2002.
[71] S. Pirandola, U. L. Andersen, L. Banchi, M. Berta, D. Bunandar, R. Colbeck, D. Englund, T. Gehring, C. Lupo, C. Ottaviani *et al.*, "Advances in quantum cryptography," *Adv. Opt. Photonics*, vol. 12, pp. 1012–1236, December 2020.
[72] N. J. Cerf, G. Leuchs, and E. S. Polzik, *Quantum Information with Continuous Variables of Atoms and Light*. London, U.K.: Imperial College Press, 2007.
[73] X.-M. Zhang, Z. Wei, R. Asad, X.-C. Yang, and X. Wang, "When does reinforcement learning stand out in quantum control? A comparative study on state preparation," *npj Quantum Inform.*, vol. 5, no. 1, p. 85, Nov. 2019.
[74] D. M. Reich, M. Ndong, and C. P. Koch, "Monotonically convergent optimization in quantum control using krotov's method," *J. Chem. Phys.*, vol. 136, no. 10, Mar. 2012.
[75] S. Akcay, D. Ameln, A. Vaidya, B. Lakshmanan, N. Ahuja, and U. Genc, "Anomalib: A deep learning library for anomaly detection," in *Proc. IEEE Int. Conf. Image Process. (ICIP)*, Bordeaux, France, Oct. 2022, pp. 1706–1710.
[76] J. Weinbub and D. Ferry, "Recent advances in Wigner function approaches," *Appl. Phys. Rev.*, vol. 5, no. 4, p. 041104, Oct. 2018.
[77] M. Everingham, L. V. Gool, C. K. I. Williams, J. Winn, and A. Zisserman, "The pascal visual object classes (VOC) challenge," *Int. J. Comput. Vis.*, vol. 88, no. 2, pp. 303–338, Sep. 2009.
[78] Z. Wang, A. C. Bovik, H. R. Sheikh, and E. P. Simoncelli, "Image quality assessment: From error visibility to structural similarity," *IEEE Trans. Image Process.*, vol. 13, no. 4, pp. 600–612, Apr. 2004.
[79] M. P. Dubuisson and A. K. Jain, "A modified Hausdorff distance for object matching," in *Proc. IEEE Int. Conf. Pattern Recognit. (ICPR)*, Jerusalem, Israel, Oct. 1994, pp. 566–568.
[80] E. del Valle, S. Zippilli, F. P. Laussy, A. Gonzalez-Tudela, G. Morigi, , and C. Tejedor, "Two-photon lasing by a single quantum dot in a high-Q microcavity," *Phys. Rev. B*, vol. 81, p. 035302, Jan. 2010.
[81] A. Vivas-Viaña and C. S. Muñoz, "Two-photon resonance fluorescence of two interacting nonidentical quantum emitters," *Phys. Rev. Res.*, vol. 3, p. 033136, Aug. 2021.
[82] K. A. Fischer, R. Trivedi, and D. Lukin, "Particle emission from open quantum systems," *Phys. Rev. A*, vol. 98, p. 023853, Aug. 2018.
[83] H. Carmichael, *An Open Systems Approach to Quantum Optics*, 1st ed. Berlin, Heidelberg: Springer-Verlag, 1993.
[84] J. C. Lagarias, J. A. Reeds, M. H. Wright, and P. E. Wright, "Convergence properties of the Nelder-Mead simplex method in low dimensions," *SIAM J. Optim.*, vol. 9, no. 1, pp. 112–147, 1998.

Syed Muhammad Abuzar Rizvi received his B.S. degree in Electrical Engineering from the National University of Sciences and Technology (NUST), Islamabad, Pakistan, in 2018. He is currently pursuing the Ph.D. degree with the Department of Electronics and Information Convergence Engineering, Kyung Hee University, South Korea. His research interests include quantum computing, quantum machine learning, quantum communication, and quantum information science.

Uman Khalid received his B.S. degree in Electronics Engineering from the Ghulam Ishaq Khan (GIK) Institute, Topi, Pakistan, in 2015, and his Ph.D. in Electronics Engineering from Kyung Hee University, South Korea, in Feb. 2023. Since Mar. 2023, he has been a Post-Doctoral Fellow with the Department of Electronics and Information Convergence Engineering, Kyung Hee University. His research interests include quantum information science, quantum metrology, and quantum networks.

Symeon Chatzinotas (Fellow, IEEE) is currently Full Professor / Chief Scientist I and Head of the research group SIGCOM in the Interdisciplinary Centre for Security, Reliability and Trust, University of Luxembourg. In parallel, he is an Adjunct Professor in the Department of Electronic Systems, Norwegian University of Science and Technology, an Eminent Scholar of the Kyung Hee University, Korea and a Collaborating Scholar of the Institute of Informatics & Telecommunications, National Center for Scientific Research "Demokritos".

In the past, he has been a Visiting Professor at EPFL, Switzerland and University of Parma, Italy and contributed in numerous R&D projects for the Institute of Telematics and Informatics, Center of Research and Technology Hellas and Mobile Communications Research Group, Center of Communication Systems Research, University of Surrey.

He has received the M.Eng. in Telecommunications from Aristotle University of Thessaloniki, Greece and the M.Sc. and Ph.D. in Electronic Engineering from University of Surrey, UK in 2003, 2006 and 2009 respectively.

He has authored more than 800 technical papers in refereed international journals, conferences and scientific books and has received numerous awards and recognitions, including the IEEE Fellowship and an IEEE Distinguished Contributions Award. He has served in the editorial board of NPJ WIRELESS TECHNOLOGY, IEEE TRANSACTIONS ON COMMUNICATIONS, IEEE OPEN JOURNAL OF VEHICULAR TECHNOLOGY and the INTERNATIONAL JOURNAL OF SATELLITE COMMUNICATIONS AND NETWORKING.

Trung Q. Duong (Fellow, IEEE) is a Canada Excellence Research Chair (CERC) and a Full Professor at Memorial University, Canada. He is also an adjunct professor at Queen's University Belfast, UK and Kyung Hee University, South Korea. He was a Distinguished Advisory Professor at Inje University, South Korea (2017-2019). His current research interests include wireless communications, quantum machine learning, and quantum optimization.

Dr. Duong has served as an Editor/Guest Editor for the IEEE TRANSACTIONS ON WIRELESS COMMUNICATIONS, IEEE TRANSACTIONS ON COMMUNICATIONS, IEEE TRANSACTIONS ON VEHICULAR TECHNOLOGY, IEEE TRANSACTIONS ON NETWORK SCIENCE AND ENGINEERING, IEEE COMMUNICATIONS LETTERS, IEEE WIRELESS COMMUNICATIONS LETTERS, IEEE WIRELESS COMMUNICATIONS, IEEE COMMUNICATIONS MAGAZINES, IEEE NETWORK and IEEE JOURNAL ON SELECTED AREAS IN COMMUNICATIONS. He received the Best Paper Award at the IEEE VTC-Spring 2013, IEEE ICC 2014, IEEE GLOBECOM 2016, 2019, 2022, IEEE DSP 2017, IWCMC 2019, 2023, 2024 and IEEE CAMAD 2023, 2024. He is the Editor-in-Chief of IEEE Communications Surveys & Tutorials and an IEEE ComSoc Distinguished Lecturer. He has received the two prestigious awards from the Royal Academy of Engineering (RAEng): RAEng Research Chair and the RAEng Research Fellow. He is the recipient of the prestigious Newton Prize 2017. He is a Fellow of the Engineering Institute of Canada (EIC), the Canadian Academy of Engineering (CAE), the Institution of Engineering and Technology (IET), and Asia-Pacific Artificial Intelligence Association (AAIA).

Hyundong Shin (Fellow, IEEE) received the B.S. degree in Electronics Engineering from Kyung Hee University (KHU), Yongin-si, Korea, in 1999, and the M.S. and Ph.D. degrees in Electrical Engineering from Seoul National University, Seoul, Korea, in 2001 and 2004, respectively. During his postdoctoral research at the Massachusetts Institute of Technology (MIT) from 2004 to 2006, he was with the Laboratory for Information Decision Systems (LIDS). In 2006, he joined the KHU, where he is now the Dean of the College of Electronics & Information as well as the College of Software. His research interests include quantum information science, wireless communication, and machine intelligence. Dr. Shin received the IEEE Communications Society's Guglielmo Marconi Prize Paper Award and William R. Bennett Prize Paper Award. He served as the Publicity Co-Chair for the IEEE PIMRC and the Technical Program Co-Chair for the IEEE WCNC and the IEEE GLOBECOM. He was an Editor of IEEE TRANSACTIONS ON WIRELESS COMMUNICATIONS and IEEE COMMUNICATIONS LETTERS.